Revealing charge carrier dynamics in squaraine:[6, 6]-phenyl-C 71-butyric acid methyl ester based organic solar cells

Aniket Rana, Chhavi Sharma, Deepak D. Prabhu, Mahesh Kumar, Yoosaf Karuvath, Suresh Das, Suresh Chand, and Rajiv K. Singh

Citation: AIP Advances **8**, 045302 (2018); doi: 10.1063/1.5018253
View online: https://doi.org/10.1063/1.5018253
View Table of Contents: http://aip.scitation.org/toc/adv/8/4
Published by the American Institute of Physics

Revealing charge carrier dynamics in squaraine: [6, 6]-phenyl-C 71-butyric acid methyl ester based organic solar cells

Aniket Rana,[1,2] Chhavi Sharma,[1,2] Deepak D. Prabhu,[3] Mahesh Kumar,[1,2] Yoosaf Karuvath,[3] Suresh Das,[3] Suresh Chand,[1,2] and Rajiv K. Singh[1,2,a]
[1]*CSIR-National Physical Laboratory, Dr. K.S. Krishnan Marg, New Delhi 110012, India*
[2]*Academy of Scientific and Innovative Research (AcSIR), CSIR-NPL Campus, New Delhi 110012, India*
[3]*CSIR-National Institute for Interdisciplinary Science and Technology, Thiruvananthapuram 695 019, Kerala, India*

(Received 5 December 2017; accepted 6 March 2018; published online 3 April 2018)

Ultrafast charge carrier dynamics as well as the generation of polaron pair in squaraine (SQ) and squaraine:[6,6]-phenyl-C 71-butyric acid methyl ester (SQ:$PCBM_{71}$) have been studied using ultrafast transient absorption spectroscopy (UTAS). The current study reveals that the pure SQ exhibits the creation of singlet and triplet states; however, incorporation of $PCBM_{71}$ in SQ results in the formation of polaron pairs with ~550ps lifetime, which in turn leads to the creation of free electrons in the device. We show that the considerable increment in monomolecular and bimolecular recombination in SQ:$PCBM_{71}$ compared to pure SQ which describes the interfacial compatibility of SQ and $PCBMC_{71}$ molecules. The present work not only provides the information about the carrier generation in SQ and SQ:$PCBM_{71}$ but also gives the facts relating to the effect of $PCBM_{71}$ mixing into the SQ which is very significant because the SQ has donor-acceptor-donor (D-A-D) structure and mixing one more acceptor can introduce more complex recombinations in the blend. These findings have been complimented by the charge transport study in the device using impedance spectroscopy. The various important transport parameters are transit time (τ_t), diffusion constant (D_n), global mobility (μ) and carrier lifetime (τ_r). The values of these parameters are 26.38 μs, 4.64×10^{-6} cm^2s^{-1}, 6.12×10^{-6} $cm^2V^{-1}s^{-1}$ and 399 μs, respectively. To the best of our knowledge such study related to SQ is not present in the literature comprehensively. https://doi.org/10.1063/1.5018253

INTRODUCTION

Organic solar cell (OSC) is a fast emerging technology as an effective alternative to the conventional inorganic photovoltaic due to its inherent advantages such as cost effectiveness, flexibility, large area possibility, ease of fabrication, etc.[1–3] Recently Heliatek has achieved 13.2% efficiency in the multi-junction solar cell.[4] However, maintaining high stability and efficiency together is still a great challenge for the commercialization of OSC. To achieve this goal, it is essential to understand the physics of charge carrier dynamics at femtosecond timescale. This paper is an attempt in this direction.

Recently use of SQ in OSC devices has gained a great momentum because of some advantages, over other donor polymers, such as easy synthesis process, being mono-dispersive in nature, easily tunable band gap, modulation of photophysical properties by changing the side group (R groups),[5]

[a]Email: rajivsingh@nplindia.org, aniket.rana@gmail.com

thermally and optically stable, absorption spectrum ranging from visible to near-infrared spectral region,[6–8] etc. Even though it is being used in the fabrication of OSC devices, yet the literature lack studies on its photophysical and carrier dynamics which is an important aspect to enhance further the efficiency and stability of these devices. Keeping this in view we have performed electro-optical and electrical measurements such as ultrafast transient absorption spectroscopy, impedance spectroscopy and current-voltage (J-V) characteristics in pure SQ films as well as SQ:$PCBM_{71}$ blends. These important studies will be proved immensely useful in designing efficient and stable SQ based OSCs.

EXPERIMENTAL METHODS

Ultrafast transient absorption spectroscopy

Thin films of SQ and SQ:$PCBM_{71}$ were spin-coated on quartz glass plate for UV-Vis and ultrafast transient absorption spectroscopy experiments. For this SQ and SQ: $PCBM_{71}$ solutions were prepared separately with the concentration 5 mg/ml. The Ti:Sapphire femtosecond laser was employed to pump and probe the samples. The ultrafast transient absorption spectrometer (Ultrafast systems, Helios) was integrated to the amplified Ti:Sapphire laser (Coherent, Legend) and an oscillator (Coherent, Micra) for the investigation of carrier relaxation dynamics. The generated output of Micra (800 nm, 80 MHz, and 45 fs) was fed to the regenerative amplifier pumped by Verdi (diode pumped solid state laser) and coupled to the stretcher/compressor gratings. The output of laser pulse having 800 nm and 45 fs pulse width with 1 kHz repetition rate and 4mJ average energy output was used. The 50% of the output was fed into the optical parameter amplifier (TOPAS, Light Conversion) for generation of the appropriate wavelength. Out of this, 25% was used to produce the white light range through a Sapphire disk for the probe pulse; residual 25% was used for higher harmonic generation. The OPA produces a 190-2600 nm femtosecond pulse with 70 fs to pump the sample. To obtain the difference spectra (ΔA) signal, the pump signal was halved to 500 Hz from the chopper. The highly stable 450 nm pump beam has been used to excite the carriers in the samples. Measuring the pump-induced changes in the optical constants (such as reflectivity or transmission of the sample) as a function of time delay between the arrival of pump and probe pulses yielded information about the relaxation of electronic states in the sample. It measures the lifetime of electronic excitations with femtosecond time resolution.

Device fabrication

Patterned ITO coated glass was cleaned by ultrasonic treatment with detergent, de-ionized water, acetone isopropyl alcohol each for 10 minutes and then dried with nitrogen air flow. After this step, the substrate was kept for UV-Ozone treatment for 5 minutes. The active material solution was prepared by dissolving SQ:$PCBM_{71}$ in 1:6 weight ratio in chloroform with 20mg/ml and kept overnight on a magnetic stirrer for mixing. Subsequently, it was spin-coated over 8nm MoO_3 deposited indium tin oxide (ITO) substrate at 1000 rpm in the nitrogen filled glove box. The 100 nm Al cathode was thermally deposited at 0.2 Å/s. The active area of the device was $6mm^2$. The basic device structure[9–11] with energy band diagram is given in figure S1 of the supplementary material.

Impedance spectroscopy

For the impedance measurement PGSTAT-30 with 1MHz to 100Hz AC sine wave signal with 100 mV amplitude was applied. The logarithmic frequency step was used to stable data at high frequency. For the fitting of all impedance data, NOVA 2.0 software was used.

RESULT AND DISCUSSION

Figure 1 shows the absorption spectrum of SQ film and SQ:$PCBM_{71}$ blend film, respectively. The SQ has a broad absorption spectral range from 500 nm to 800 nm, covering both the visible as well as part of initial infrared (IR) spectrum. The absorption peak around 627 nm and one shoulder peak at 654 nm indicate the crystalline domain formation in the film. When SQ is blended with $PCBM_{71}$ the absorption spectrum shows peak at 538 nm and the signature SQ peak at 693 nm with red-shift due to

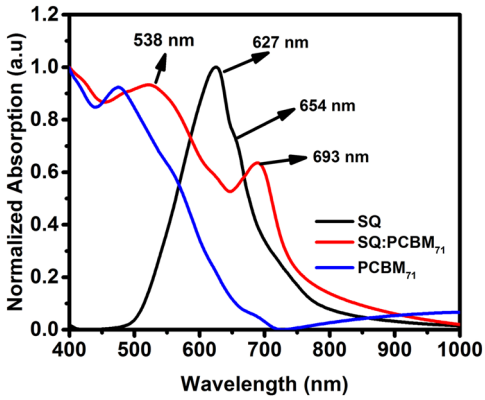

FIG. 1. UV-Vis absorption spectrum of SQ (black line), SQ:$PCBM_{71}$ (red line) and $PCBM_{71}$ (blue line) film on quartz glass substrate after annealing at 110 °C.

J-aggregation which is due to exciton coupling of the SQ in the $PCBM_{71}$ and interchain interactions in the solid film.[12]

In figure 2 photoluminescence spectrum is given for SQ and SQ:$PCBM_{71}$ film with chemical structure. The excitation wavelength is 500 nm for photoluminescence measurement. A sharp quenching in SQ photoluminescence peak (685 nm) is observed, and it refers to the efficient exciton to polaron formation in the presence of $PCBM_{71}$. In the blend strong quenching can occur due to SQ itself (self-quenching) and by the $PCBM_{71}$ as well. SQ can be considered as fluorophore either to SQ itself or $PCBM_{71}$. In the SQ:$PCBM_{71}$ blend system SQ may bind with $PCBM_{71}$ or with another SQ molecule to allow self-quenching as the J-aggregation suggested by the red shift in the absorption spectra. The self-quenching of SQ and the quenching in the presence of PCBM study by Bi Zhu et al.[13] reveals that there is an increase in the Stern-Volmer constant[14] as the concentration of PCBM is increased in the SQ.[15] It was concluded that PCBM and SQ complex is formed with the increase in the PCBM concentration. In the present case $PCBM_{71}$ is six times higher than SQ therefore the aggregation in SQ takes place probably due to the phase separation at the interface. Further, the much deeper aspect of SQ and $PCBM_{71}$ interaction has been revealed through UTAS study.

Photophysics of SQ and SQ:$PCBM_{71}$ blended films by UTAS

The charge carrier dynamics of SQ and SQ:$PCBM_{71}$ blend in picosecond time scale (Figure 3(a–b)) has been carried out with the help of ultrafast transient absorption spectroscopy in the range of 100fs to 1 ns. For this, the probe delay was covering the visible to NIR region. The data was plotted on a semi-logarithmic scale to identify prominent peaks at low wavelength scale

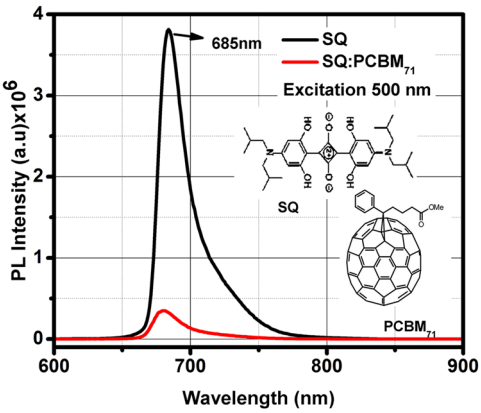

FIG. 2. Photoluminescence spectra of pristine SQ (black line) and SQ:$PCBM_{71}$ (red line) blend films excited at 500 nm. Inset shows the schematic of chemical structure of SQ and $PCBM_{71}$.

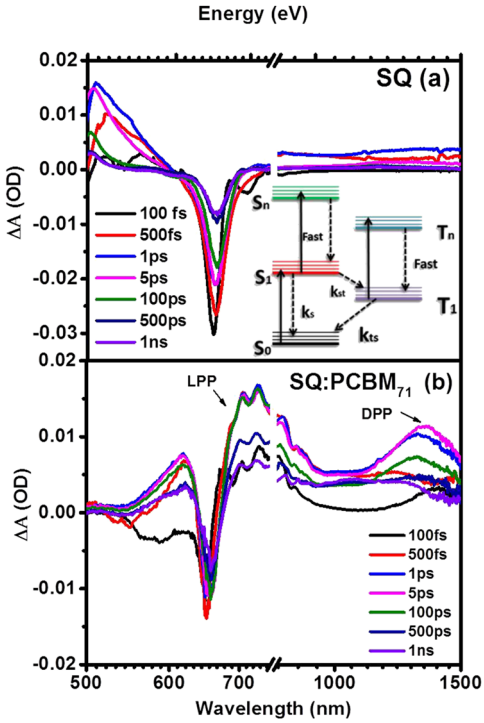

FIG. 3. The relative differential absorption (ΔA(OD)) spectra for (a) SQ film (b) SQ:$PCBM_{71}$ film on quartz substrate at 100 fs, 500 fs, 1ps, 5ps, 100 ps, 500 ps, and 1000 ps probe delay in visible to NIR region. The LPP and DPP stands for localized polaron pair and delocalized polaron pair.

as well. The pump wavelength is selected at 480nm according to SQ and SQ:$PCBM_{71}$ absorption to avoid detection of pump pulse by the probe. It is observed that high molar extinction coefficient of SQ dyes caused multiple excitations in a single polymer strand. Therefore, to avoid multiple excitations, the pump energy was kept very low (45 μJ/cm^2). In figure 3(a) the negative differential absorption (ΔA<0) appears in the range of ~600 nm to ~680 nm with a peak at ~650nm. It has been attributed to photobleaching of ground state carriers termed as ground state bleaching (GSB) signal.[16] At ~100 fs probe delay with respect to the pump, the GSB signal strength is maximum and then reduces progressively with higher probe time delay. It has been assigned to the decay of excited carriers to the ground state carriers. The positive differential absorption (ΔA>0) originates due to photoinduced absorption (PIA) of the excited state carriers and absorption of the photo products.[16,17] The PIA signal appears at ~500 nm in SQ due to the excitation of initial band edge electrons to higher states (S_1 to S_n). The second PIA signal from ~750 nm onwards remains flat and feeble up to deep IR region. The self-quenching[18] of charge carriers prohibits the creation of free polaron pair in pure SQ due to the donor-acceptor-donor (D-A-D) arrangement in the SQ[19] shown in the inset of figure 2. Therefore, no significant signature of long lived charge carrier species in a pure SQ was observed in the photoinduced absorption which is revealed by the multicomponent fitting in figure 4(a). Inset of figure 3(a) shows the transitions in the energy levels for SQ highlighting the excitation and decay mechanism of charge carriers. The UTAS data can estimate the singlet and triplet states in SQ by correlating the charge carrier excitation and decay mechanism. Therefore, the strong GSB signal at ~650 nm corresponds to S_0 to S_1 transition[19] whereas the PIA at ~500 nm occurs subsequently due to S_1 to S_n transition.

The interaction of SQ and $PCBM_{71}$ is clearly evident in UV-Vis and photoluminescence spectrum in figure 1 and figure 2. The signature excitonic peak of SQ has been redshifted to ~693 nm which is due to the formation of J-aggregates in the mixture.[20] The SQ and $PCBM_{71}$ interaction and the decay dynamics of charge carriers in the SQ:$PCBM_{71}$ blend can be explained in terms of the origin of excitation and fundamental charge carrier species in pure SQ.

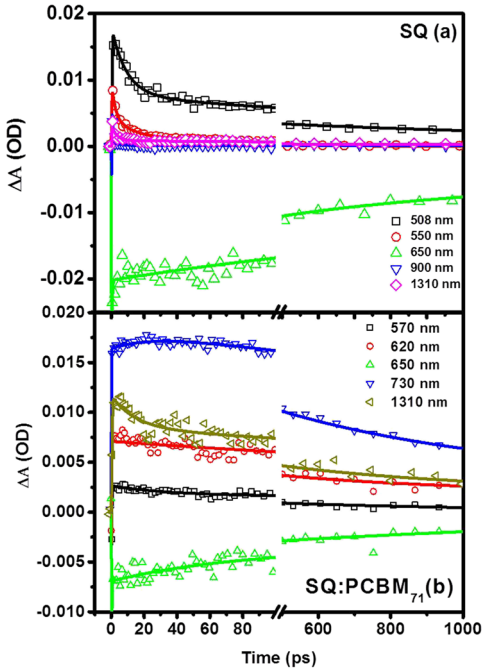

FIG. 4. The GSB and PIA decay kinetics of associated charge carriers for (a) SQ, (b) SQ:$PCBM_{71}$ blend. The dotted line corresponds to experimental data whereas continuous line relates to the exponential fit at significant wavelengths for the charge carrier formation and transition according to the relative differential absorption (ΔA(OD)) spectra given in figure 3(a–b).

The formation of exciton and polaron in SQ:$PCBM_{71}$ is observed in figure 3(b). At ~100 fs probe delay, GSB signal appears instead of PIA signal due to excitation of S_0 (ground state) until this time period. The S_1 to S_n transition PIA peak has been red-shifted from ~500nm to ~600nm in the SQ:$PCBM_{71}$ blend with respect to the pure SQ. It establishes the interaction of $PCBM_{71}$ with SQ leading to the J-aggregation at the molecular level in the SQ:$PCBM_{71}$ blend. While a strong GSB signal is also present in the blend but the maximum bleach signal is achieved at ~500fs probe delay, which occurs at 100 fs in the SQ. The delay in the GSB by about 400 fs is due to the transfer of holes into the highest occupied molecular level (HOMO) of SQ from $PCBM_{71}$ as the concentration of fullerene is very high. Two significant PIA signals appear in transient spectra at ~730 nm and ~1330 nm, respectively. Within few femtoseconds to picosecond (~100 fs to ~100 ps), after the excitation of SQ:$PCBM_{71}$ blend, the creation of exciton charge transfer state occurs at the donor-acceptor interface. The first PIA signal at ~730 nm has been attributed to the localized polaron pair in SQ:$PCBM_{71}$ blend.[21,22] These localized polaron pairs are converted into delocalized polaron pair and produce free charge carriers in the blend which can be observed at ~1 ps to ~100 ps time scale. The presence of delocalized polaron pairs found at ~1330 nm also directly contribute to free charge carriers in the blend.

Charge carrier dynamics and time-based examination of SQ and SQ:$PCBM_{71}$ at significant wavelengths according to figure 3(a–b) can be analyzed from decay kinetics shown in figure 4(a–b). All these kinetics explain the excitation and decay of the charge carriers as well as interaction of SQ and $PCBM_{71}$. For the clear depiction of fitting, the time axis of the plotted data has been divided into small (0-100 ps) and larger (500-1000 ps) time scale, respectively. Both the GSB and PIA signal is best fitted with a sum of three exponential functions given in equation (1).

$$\Delta OD\,(t) = A_1 \exp\,(-\,t/\tau_1) + A_2 \exp\,(-\,t/\tau_2) + A_3 \exp(-\,t/\tau_3) \quad (1)$$

Where τ_1 represents the vibrational relaxation to the closest lower state which is fast in nature, τ_2 represents the radiative or non-radiative decay of the excited charge carriers to the ground state,[23] and τ_3 represents the triplet state transition after the intersystem crossing which has long decay time due.[24]

The lifetime of excited charge carrier in SQ at ~508 nm is ~120 ps and has been identified as singlet states. Some of these singlet state charge carriers at S_1 transferred to the triplet state (T_1) through intersystem crossing mechanism with $1/\tau_{st}$ (inset of figure 3(a)) the rate constant. The trailing edge of PIA signal in SQ at ~550 nm shows the fast transition of singlet to triplet state within ~13 ps. After the decay in the PIA signal, within ~228 ps the fast recovery of bleaching signal at ~650 nm shows the transition of electrons from S_1 to S_0 states. It shows the formation of singlet state within SQ dye. Therefore, the lifetime of S_1 state can be estimated[25,26] from equation (2)

$$\tau_{s1} = 1/(1/\tau_s + 1/\tau_{ts}) \quad (2)$$

The estimated lifetime of S_1 from above equation is ~12 ps. Enough lifetime of the singlet state and full recovery of the bleach signal shows the existence of intersystem crossing in SQ which indicates the probability of the creation of triplet states in SQ. The decay time of PIA transient signal at ~900 nm (Figure 4(a)) is ~0.2 ps indicating short-lived charge species in SQ whereas at ~1300 nm some delocalized polaron pairs are available with a decay time constant ~271 ps. The time constant τ_3 is neglected here as the amplitude of A_3 is very small.

The charge transfer from SQ to $PCBM_{71}$ further confirmed the formation of polaron pairs that have been analyzed through the temporal analysis of decay kinetics of relative differential absorption. While analyzing the relative differential absorption spectra, it is observed that there is a red shift in the S_1 to S_n transition PIA peak from ~500 nm to ~600 nm due to the blending of SQ and $PCBM_{71}$. Due to the J-aggregation network SQ:$PCBM_{71}$, the lifetime of the singlet states in the SQ:$PCBM_{71}$ blend at ~620 nm increases up to 355 ps from 120 ps compared to the pure SQ. The decay time of GSB has reduced significantly to ~70 ps from ~228 ps due to the charge transfer state occurring at the donor-acceptor interface. The significant rise in triplet state up to 3.8ns is observed. These long excitonic states generate the polaron pairs in SQ:$PCBM_{71}$ blend. The first PIA peak after the recovery of bleaching occurs at ~730 nm has a decay time of 593 ps. These localized polarons at 730 nm further get delocalized in the SQ $PCBM_{71}$ network and contribute to the free charge carriers. These delocalized polarons have a peak at ~1330 nm with decay time 529 ps. All the decay time constant for SQ and SQ:$PCBM_{71}$ with their pre-exponential factors has been listed in Table I and Table II.

Recombination or permanent degradation of charge carriers takes place after the photoexcitation via monomolecular and bimolecular processes in the both pure SQ film and SQ:$PCBM_{71}$ blend.[27,28] The study of recombination model can describe the effect of $PCBM_{71}$ mixing in SQ. The Langevin recombination process describes the bimolecular process which happens when two free opposite

TABLE I. The lifetime of excited and associated amplitude for pure SQ film after fitting.

Wavelength, nm	508 nm	550 nm	650 nm	900 nm	1300 nm
A_1	0.544	0.512	-0.633	-0.57	0.707
τ_1 (ps)	9	2.15	0.266	0.145	3.3
A_2	0.185	0.365	-0.142	0.429	0.303
τ_2 (ps)	120	13.2	228	0.16	271
A_3	0.271	0.123	-0.225	0.000233	0.015
τ_3 (ps)	1450	245	2020	5.5	275

TABLE II. The lifetime of excited carriers and associated amplitude for SQ:$PCBM_{71}$ after fitting.

Wavelength, nm	620 nm	650 nm	730 nm	1310 nm
A_1	0.914	-0.958	0.200	0.366
τ_1 (ps)	0.0675	0.069	25.8	14.7
A_2	0.0483	-0.0165	0.79	0.623
τ_2 (ps)	355	70.3	593	529
A_3	0.0378	-0.0255	0.010	0.011
τ_3 (ps)	3670	1320	1530	1600

TABLE III. The recombination pre-factor and rates for the SQ and SQ:$PCBM_{71}$ sample calculated at GSB.

Sample	$k_1(s^{-1})$	$k_2(s^{-1})$	α	f
SQ	2.0	0.15	0.1	0.02
SQ:$PCBM_{71}$	2.92	0.54	0.02	0.01

charges carriers recombine and having originated from the separate excitons. The monomolecular recombination is best described through trap assisted recombination at the interface. Both types of recombination occur independently if the fraction (f) experience bimolecular recombination. Then the remaining fraction (1-f) undergoes monomolecular recombination. If the total photogenerated carriers is N and out of the total generated carriers N_0 goes through bimolecular and monomolecular recombination process, which can be described by the following equation (3)[29]

$$\frac{N}{N_0} = ((1-f)^{-\alpha} + k_1 t)^{-1/\alpha} + (f^{-(\alpha+1)} + k_2 t)^{-1/(\alpha+1)} \tag{3}$$

Where α is the concentration dependent exponent and $k_1 = \alpha\beta_1 N_0^{\alpha}$ and $k_2 = (\alpha+1)\beta_2 N_0^{(\alpha+1)}$, here β_1 and β_2 are recombination pre-factors for monomolecular and bimolecular recombination process and k_1 and k_2 are the recombination rates for monomolecular and bimolecular, respectively. The GSB is very useful in identifying the several species present in the sample therefore, above equation (3) has been fitted in MATLAB and estimated parameters listed in Table III to categorize the above mentioned recombination rates (k_1 and k_2) for SQ and SQ:$PCBM_{71}$, respectively. Both the mono molecular recombination rate (k_1) and bimolecular recombination rate (k_2) have increased after mixing $PCBM_{71}$ in SQ. This shows the creation of trap states at the phase separation interface of SQ and $PCBM_{71}$. Table III shows the recombination pre-factor and rates for the SQ and SQ:$PCBM_{71}$ samples, respectively. From the above study, various fundamental facets have been revealed such as the creation of singlet states and their conversion to the triplet state and the polaron pair is generated in SQ:$PCBM_{71}$ within ~1 to ~100 ps after the pump excitation and decays within ~500 ps.

SQ:$PCBM_{71}$ solar cell device fabrication and electrical characterization

The photophysical properties, charge carrier generation and recombination of pure SQ and SQ:$PCBM_{71}$ (1:6) blend have been explained in the previous sections.[30–33] The similar blend ratio has been used to fabricate the device. Therefore, the electrical parameters according to the current voltage characteristics given in figure 5, can be related to the photophysical properties of the active material. The fabricated device demonstrates the 2.4% power conversion efficiency (η) with 0.62 V open circuit voltage (V_{oc}), and 10.7mA/cm^2 short-circuit current (J_{sc}). The dark parameter like the ideality factor (n) and reverse saturation current (J_0) is 3 and 2.1x10^{-4} mA/cm^2, respectively. The other

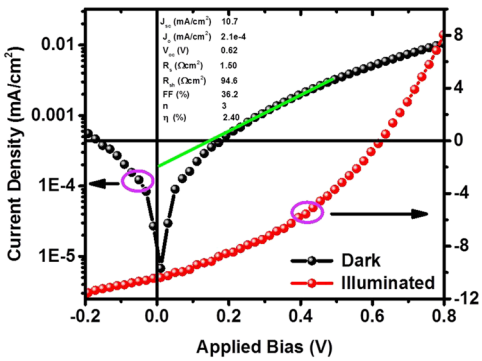

FIG. 5. Current density vs. applied bias (J-V) curve plot for the fabricated solar cell. Left side Y-axis corresponds to the dark current density whereas right side Y-axis corresponds to the illuminated current density. Dark J-V characteristics (Black line) have been plotted in semi-logarithmic scale and the illuminated J-V characteristics (Red line) plotted in normal scale. The inset shows the device parameters evaluated from dark and light J-V characteristics.

device parameters like fill factor (FF), series resistance (R_s) and shunt resistance (R_{sh}) are 36.2, 1.50 Ωcm^2 and 94.6 Ωcm^2 respectively. In essence, the above studies establish the photophysics/charge carrier dynamics in SQ:$PCBM_{71}$ based OSCs and scope of suitable modulation of these properties in new blends for improving further the efficiency and stability of these devices using these emerging cost-effective combinational donor acceptor materials.

Impedance spectroscopy and charge carrier transport parameter evaluation

Further, the fabricated devices have been examined through impedance spectroscopy to understand kinetics governing phenomenon like recombination in the device, mobile carrier lifetime, transit time and mobility of majority carriers based on the parameters extracted from the equivalent circuit after fitting. The DC equivalent circuit shown in inset of figure 6(a) comprising R_S originated from the device contact resistance and resistance from measuring wires. The value for series resistance estimated from the impedance is almost similar to the calculated from J-V characteristics. The first $R_t||CPE_t$ combination is originated from the contact and transport effect whereas R_t is transport resistance. Accordingly, the characteristics transit time (τ_t) across the device can be calculated through expression[34] i.e.

$$\tau_t = R_t C_t \tag{4}$$

where $C_t = (R_t Q)^n / R_t$. Measurement of transit time at short circuit under illumination can give the mobility of majority charge carriers through the following relation[35,36]

$$\mu = d^2 / V_{oc} \tau_t \tag{5}$$

where d is active layer thickness (~100 nm) and V_{oc} is the open circuit voltage. Another important parameter which can be estimated from impedance is recombination resistance (R_r) and chemical capacitance ($C\mu$). Later one is related to the increase in the charge (Q) and carrier density (n) with the variation in the quasi-Fermi level (E_f), $C\mu = q(dQ/dE_f)$.[37] The current flows through the R_r in the DC equivalent circuit is referred as recombination current. The value of R_r biased at open circuit voltage can give the cell characteristic response time, which can also be referred as mobile carrier lifetime recombination time.[36,38–40]

$$\tau_r = R_r C_\mu \tag{6}$$

Transport time is usually 2 to 3 order faster compared to the recombination lifetime. Diffusion constant (D_n)[34,36] of the electron, can be calculated from the following relation

$$D_n = d^2 / \tau_t \tag{7}$$

The Nyquist plot for the fabricated device under a dark condition with varying forward bias from 0.0 V to 0.5 volts is shown in figure 6(a). The change in the value of R_r before built-in bias (0 to 0.1 V) is small, but as the device moves into the forward bias region significant difference appears in the recombination resistance due to the reduction in the junction potential at the donor-acceptor interface. The recombination time reduces with the increment in the bias voltage whereas average transit time ($\tau_{t\,avg}$ 21.712 μs) and diffusion constant ($D_{n\,avg}$ 4.64×10^{-6} $cm^2 s^{-1}$) of electrons are almost similar with the bias voltage which can be observed in table S1 (supplementary material). The Nyquist plot in the illuminated condition (figure 6(b)) at the short circuit and the open circuit conditions can be used for the calculation of mobility and carrier lifetime from the equation (6–7). Therefore the calculated value of mobility (μ) is $6.12 \times 10^{-6} cm^2 V^{-1} s^{-1}$ and average mobile carrier lifetime (τ_r) is 399 μs are consistent with the long lifetime of polaron pairs in the SQ:$PCBM_{71}$. Figure 6(c–d) shows the frequency response of the device impedance on the semi-logarithmic plot. Unlikely the Nyquist plot, the Bode plot shows the frequency dependent information and discloses important low impedance behavior observed at high frequencies. The slope at the transition between low and high frequency asymptotes can give important information regarding the nature of impedance response and characteristics frequency (f_c, the frequency at the highest peak in Nyquist plot). Bode plot representation utility is in the circuit analysis. The Phase angle plot is sensitivity to the system parameter hence it gives a good confidence regarding the selection of circuit model and fitting to the experimental data. Therefore, around 1000Hz device makes a transition from capacitive to resistive nature. In fact, lower than this slope current start flowing through predominantly due to the resistor and phase angle approaches to zero.

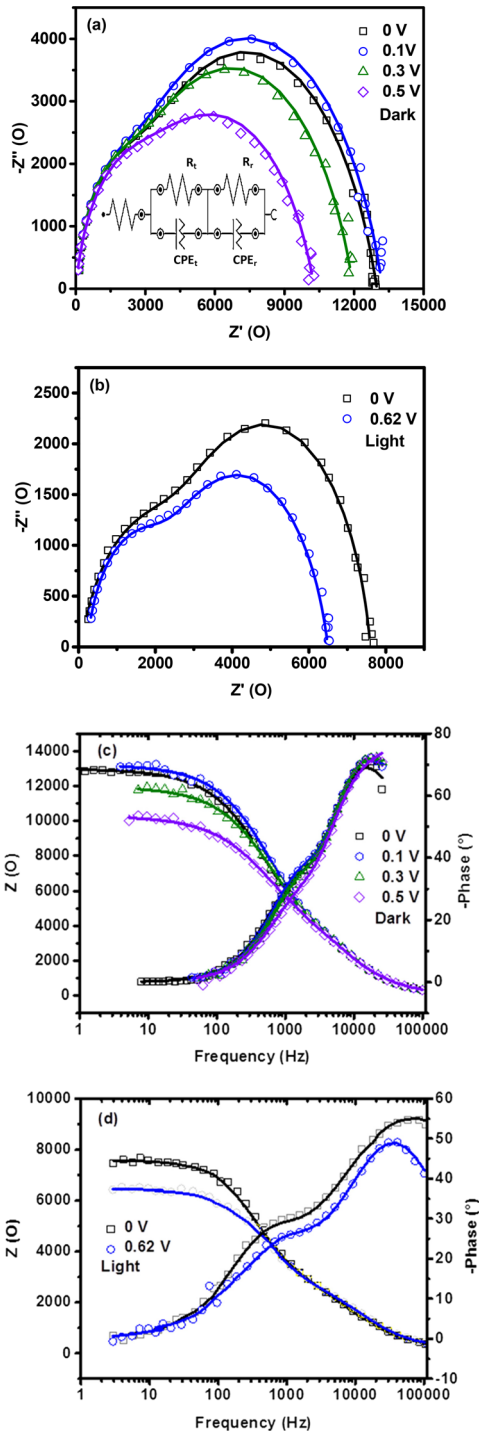

FIG. 6. Impedance response of SQ:$PCBM_{71}$ device (a) under dark condition at 0.0 to 0.5 V. Inset shows equivalent circuit used for fitting the experimental data. (b) under 100 mW white light illuminated condition for 0.0V and at V_{oc} (0.62V) (c) bode plot under dark condition at 0.0 to 0.5V (d) bode plot under 100mW/cm^2 illuminated condition at short circuit condition (0.0V) and open circuit (V_{oc}) The points represent the measured data whereas solid lines represent fit respectively.

CONCLUSION

In conclusion, we have established the concept of charge carrier dynamics in organic solar cells based on SQ:$PCBM_{71}$ donor-acceptor combination by ultrafast transient absorption and impedance

spectroscopy. A strong correlation has been revealed between the generation of localized, delocalized and subsequently free polarons. The transient study establishes the creation as well as the decay of singlet and triplet states in pure SQ material. However, the formation of polaron pairs with ~550 ps lifetime is confirmed with the incorporation of $PCBM_{71}$ in pure SQ. The absorption and Photoluminescence spectra inferred the intermolecular interaction between SQ and $PCBM7_{71}$ and aggregation. Further, the increment in monomolecular and bimolecular recombination in SQ:$PCBM_{71}$ compared to the SQ clarifies the interfacial compatibility of SQ and $PCBMC_{71}$ molecules, which is crucial for efficient charge transport in organic solar cell (OSC) devices. The impedance spectroscopy has been utilized to establish the charge transport mechanism and evaluation of various important transport parameters such as transit time (τ_t), diffusion constant (D_n), mobility (μ), carrier lifetime (τ_r) in the device and their values are 21.7 μs, 0.36 nm, $6.12x10^{-6}$ $cm^2V^{-1}s^{-1}$ and 399 μs, respectively. The actual charge transport of this charge species in SQ:$PCBM_{71}$ solar cell (PCE ~2.4%) has been revealed by impedance spectroscopy. The estimated transit time (τ_t), diffusion constant (D_n), mobility (μ) and carrier lifetime (τ_r) in the device are 26.38 μs and 0.36 nm, $6.12x10^{-6}$ $cm^2V^{-1}s^{-1}$ and 399 μs, respectively. Initial efficiency of about 2.4% has been achieved in the device with conventional configuration which permits the scope of further enhancement using suitable interface engineering of charge extraction layers. In essence, these findings reveal the fundamental and applied facet in of SQ:$PCBM_{71}$ solar cell material and devices which will prove immensely beneficial for further enhancing the efficiency of the next generation devices.

SUPPLEMENTARY MATERIAL

See supplementary material for device structure with energy band diagram and calculated parameters for impedance spectroscopy.

ACKNOWLEDGMENTS

The authors are thankful to the Director, National Physical Laboratory, Dr. K. S. Krishnan Marg, New Delhi, for his kind support. The authors gratefully recognize the financial support from the project. One of us, Mr. A. Rana is thankful to University Grant Commission, New Delhi, India for the award of Senior Research Fellowship. Dr. S Chand who has been the Indian coordinator for the Indo-UK project entitled "Advancing the Production Potential and Efficiency of Excitonic solar cells (APEX)" is thankful to DST for funding this program.

[1] L. Mao, J. Tong, S. Xiong, F. Jiang, F. Qin, W. Meng, B. Luo, Y. Liu, Z. Li, Y. Jiang, C. Hernandez, B. Kippelen, and Y. Zhou, J. Mater. Chem. A **5** (2017).
[2] C. Lungenschmied, G. Dennler, H. Neugebauer, S. N. Sariciftci, M. Glatthaar, T. Meyer, and A. Meyer, Solar Energy Materials and Solar Cells **91**, 379 (2007).
[3] S.-I. Na, S.-S. Kim, J. Jo, and D.-Y. Kim, Advanced Materials **20**, 4061 (2008).
[4] C. Jahnel, Heliatek, Press-Release 2 (2016).
[5] L. Hu, Z. Yan, and H. Xu, RSC Advances **3**, 7667 (2013).
[6] G. Chen, H. Sasabe, T. Igarashi, Z. Hong, and J. Kido, J. Mater. Chem. A **3**, 14517 (2015).
[7] Z. Y. Wang, R. Y. Wang, and N. Y. Fu, Chinese Journal of Organic Chemistry **31**, 415 (2011).
[8] S. H. Bae, K. D. Seo, W. S. Choi, J. Y. Hong, and H. K. Kim, Dyes and Pigments **113**, 18 (2015).
[9] S. Chen, X. Yu, M. Zhang, J. Cao, Y. Li, L. Ding, and G. Shi, J. Mater. Chem. A **3**, 18380 (2015).
[10] Irfan, H. Ding, Y. Gao, C. Small, D. Y. Kim, J. Subbiah, and F. So, Applied Physics Letters **96**, 243307 (2010).
[11] J. Meyer, S. Hamwi, M. Kröger, W. Kowalsky, T. Riedl, and A. Kahn, Advanced Materials **24**, 5408 (2012).
[12] S. F. Volker, A. Schmiedel, M. Holzapfel, K. Renziehausen, V. Engel, and C. Lambert, Journal of Physical Chemistry C **118**, 17467 (2014).
[13] B. Zhu, M.S thesis, Rochester Institute of Technology, New York (2014).
[14] N. J. B. Green, S. M. Pimblott, and M. Tachiya, The Journal of Physical Chemistry **97**, 196 (1993).
[15] C. Zheng, A. R. Penmetcha, B. Cona, S. D. Spencer, B. Zhu, P. Heaphy, J. A. Cody, and C. J. Collison, Langmuir **31**, 7717 (2015).
[16] R. Berera, R. van Grondelle, and J. T. M. Kennis, Photosynthesis Research **101**, 105 (2009).
[17] M. Scarongella, J. De Jonghe-Risse, E. Buchaca-Domingo, M. Causa, Z. Fei, M. Heeney, J. E. Moser, N. Stingelin, and N. Banerji, Journal of the American Chemical Society **137**, 2908 (2015).
[18] A. Wojcik, R. Nicolaescu, P. V. Kamat, Y. Chandrasekaran, and S. Patil, Journal of Physical Chemistry A **114**, 2744 (2010).
[19] P. V. Kamat, S. Das, K. G. Thomas, and M. V. George, The Journal of Physical Chemistry **96**, 195 (1992).
[20] Y. T. Fu, D. A. Da Silva Filho, G. Sini, A. M. Asiri, S. G. Aziz, C. Risko, and J. L. Brédas, Advanced Functional Materials **24**, 3790 (2014).

[21] N. Zarrabi, P. L. Burn, P. Meredith, and P. E. Shaw, Journal of Physical Chemistry Letters **7**, 2640 (2016).
[22] A. De Sio, F. Troiani, M. Maiuri, J. Réhault, E. Sommer, J. Lim, S. F. Huelga, M. B. Plenio, C. A. Rozzi, G. Cerullo, E. Molinari, and C. Lienau, Nature Communications **7**, 13742 (2016).
[23] A. L. Ayzner, S. C. Doan, B. Tremolet De Villers, and B. J. Schwartz, Journal of Physical Chemistry Letters **3**, 2281 (2012).
[24] A. Köhler and H. Bässler, Materials Science and Engineering R: Reports **66**, 71 (2009).
[25] S. Webster, D. Peceli, H. Hu, L. A. Padilha, O. V. Przhonska, A. E. Masunov, A. O. Gerasov, A. D. Kachkovski, Y. L. Slominsky, A. I. Tolmachev, V. V. Kurdyukov, O. O. Viniychuk, E. Barrasso, R. Lepkowicz, D. J. Hagan, and E. W. Van Stryland, Journal of Physical Chemistry Letters **1**, 2354 (2010).
[26] S. N. R. Swatton, K. R. Welford, R. C. Hollins, and J. R. Sambles, Applied Physics Letters **71**, 10 (1997).
[27] B. Wu, X. Wu, C. Guan, K. F. Tai, E. Kok, L. Yeow, H. J. Fan, N. Mathews, and T. C. Sum, Nat Commun. **4**, 2004 (2013).
[28] B. N. Tessler, Y. Preezant, N. Rappaport, and Y. Roichman, Advanced Materials **21**, 2741 (2009).
[29] A. Rana, N. Gupta, A. Lochan, G. D. Sharma, S. Chand, M. Kumar, and R. K. Singh, Journal of Applied Physics **120** (2016).
[30] P. C. R. Varma and M. A. G. Namboothiry, Phys. Chem. Chem. Phys. **18**, 3438 (2016).
[31] G. Wei, S. Wang, K. Sun, M. E. Thompson, and S. R. Forrest, Advanced Energy Materials **1**, 184 (2011).
[32] G. D. Wei, S. Y. Wang, K. Renshaw, M. E. Thompson, and S. R. Forrest, ACS Nano **4**, 1927 (2010).
[33] Q. Yang, D. Yang, S. Zhao, Y. Huang, Z. Xu, X. Liu, W. Gong, X. Fan, Q. Huang, and X. Xu, Applied Surface Science **284**, 849 (2013).
[34] G. Garcia-Belmonte, A. Munar, E. M. Barea, J. Bisquert, I. Ugarte, and R. Pacios, Organic Electronics **9**, 847 (2008).
[35] A. Kokil, K. Yang, and J. Kumar, Journal of Polymer Science, Part B: Polymer Physics **50**, 1130 (2012).
[36] J. I. Basham, T. N. Jackson, and D. J. Gundlach, Advanced Energy Materials **4**, 1400499 (2014).
[37] A. Rana, R. Baronia, R. Pasricha, and R. K. Singh, Materials Research Express **1**, 45506 (2014).
[38] J. Bisquert, Journal of Physical Chemistry B **106**, 325 (2002).
[39] F. Fabregat-Santiago, G. Garcia-Belmonte, I. Mora-Seró, and J. Bisquert, Physical Chemistry Chemical Physics: PCCP **13**, 9083 (2011).
[40] H. Kurt and C. W. Ow-Yang, Physica Status Solidi (A) Applications and Materials Science **213**, 3165 (2016).